Space weather forecasting using SARIMA

Mina Baniamein, *Mission Analysis Engineer, Capsule Corporation Srl*

***Abstract*—Solar fluxes and geomagnetic activity influence the temperature of the air, and consequently the density. These phenomena are hard to predict because of their highly nonlinear and stochastic nature. However, they have significant effects on LEO space missions and orbital decay time estimations, since air drag is one of the major perturbations in this region. Inaccurate density estimates can indeed result in substantial errors in SmallSat mission operations-related quantities, such as station-keeping delta-v budgets, and compliance with mission disposal requirements that are getting stricter due to the growing amount of space debris.**

This study addresses the problem of forecasting future atmospheric conditions by focusing on the prediction of key space weather indicators. Historical time series of the F10.7 solar radio flux and the Ap geomagnetic index are analyzed using a Seasonal Autoregressive Moving Average (SARIMA) modeling approach. This technique is selected for its ability to represent both long-term trends and recurring seasonal patterns embedded in the data. The resulting forecasts are expressed as probabilistic ranges rather than single-point estimates, allowing uncertainty to be explicitly quantified.

The predicted indices are then used to derive corresponding atmospheric density values, which can be directly employed in preliminary mission design activities. The proposed methodology is demonstrated through representative LEO use cases, including the estimation of station-keeping delta-v requirements and the assessment of orbital decay times. Results are evaluated with respect to European Cooperation for Space Standardization (ECSS) guidelines, showing that the approach provides a practical and statistically sound tool for early-phase mission analysis under space weather uncertainty.

***Index Terms*—Space, weather, forecast, SARIMA, decay, station-keeping**

I. Introduction

THIS work addresses the long-term prediction of atmospheric density and thus aerodynamic drag, a primary perturbation influencing Low Earth Orbit (LEO) missions. The approach chosen was to model the density with the high-fidelity NRLMSISE00 model [1, 2] and couple it with the numerical integration of the orbital dynamics equations. A key challenge in this method is giving the correct inputs of future spacecraft state and environment to the atmospheric model. NRLMSISE00 requires data related to the time and position of the spacecraft, which are relatively simple to predict, but also the future values of:

- $F_{10.7}$: represents the daily measure of solar radio flux density at a wavelength of 10.7 cm. It has an estimated seasonal trend of 11 years.
- a_p: planetary geomagnetic index measured that quantifies the level of geomagnetic activity over 3-hour intervals on a linear scale. For every day, eight values of a_p are measured. tudies suggested a semiannual seasonality for this parameter [3].
- A_p: daily mean geomagnetic activity, which corresponds to the average of the eight 3-hourly ap values recorded within a 24-hour period.

To predict these values, depending from highly stochastic phenomena, there exist currently many approaches, ranging from statistical and regression-based models [4–6] that provide simple empirical forecasting capabilities, to physics-based frameworks, such as the Space Weather Modeling Framework [7] and ESA's uncertainty-aware tools [8], that offer high-fidelity space weather simulations. Machine learning is the state of the art, with applications by Camporeale et al. [9], ESA's DENSER project [10], and heliophysics studies [11]. The forecasting techniques applied in this work is the SARIMA (Seasonal Autoregressive Integrated Moving Average) model applied to time series formd by past solar and geomagnetic data. This is chosen as an intermediate approach between simple empirical heuristics and full physics-based models, without requiring complex models and high computational load to run, and still capturing key seasonal properties for predicting the atmospheric density in early-phases space mission analysis works.

II. SARIMA framework

SARIMA is an extension of the ARIMA (Autoregressive Integrated Moving Average) model [12] for time series characterized by recurring seasonal patterns, in this work denoted as y_t. While ARIMA accounts for autoregressive, differencing, and moving-average components, SARIMA additionally includes seasonal autoregressive, seasonal differencing, and seasonal moving-average terms. The mathematical representation of an ARIMA modeled time series is expressed as:

$$\begin{cases} \nabla^d y_t = z_t \\ \quad z_t = \delta + \phi_1 z_{t-1} + \cdots + \phi_p z_{t-p} \\ \qquad + a_t - \Theta_1 a_{t-1} - \cdots - \Theta_q a_{t-q} \end{cases} \tag{1}$$

where z_t is the differenced time series of d order, δ denotes a constant, ϕ represents autoregressive parameters and a_t corresponds to a random white noise at instant t. Similarly, Θ represents the moving average parameters.

Using the backshift operator B:

$$B^k y_t = y_{t-k} \tag{2}$$

the differenced seasonal process fitted by SARIMA can be written as

$$z_t = \nabla_s^D \nabla^d y_t = (1 - B^s)^D (1 - B)^d y_t, \tag{3}$$

M. Shell was with the Department of Electrical and Computer Engineering, Georgia Institute of Technology, Atlanta, GA, 30332 USA e-mail: (see http://www.michaelshell.org/contact.html).

J. Doe and J. Doe are with Anonymous University.

Manuscript received April 19, 2005; revised August 26, 2015.

where d and D are the non-seasonal and seasonal differencing orders, respectively. s is the seasonal period of the time series. The complete model is denoted as SARIMA$(p, d, q) \times (P, D, Q)_s$.

The appropriate SARIMA model identification follows the Box-Jenkins methodology [12], which relies on statistical tools such as the autocorrelation function (ACF), the partial autocorrelation function (PACF), and the Augmented Dickey–Fuller (ADF) test [13]. The ADF test is first used to assess stationarity and determine the required differencing orders. Then, ACF and PACF plots are analyzed to identify the non-seasonal parameters p and q, as well as the seasonal parameters P and Q. After selecting the model orders, the SARIMA model is estimated and validated through residual diagnostics, ensuring the absence of serial correlation through the Ljung-Box test [14]. It is also required to assess the type of uncertainty distribution associated with the model and the forecasts. In the first instance, the normality of distribution is assessed with the Jarque-Bera test [15]. Furtherly, heteroskedasticity of the model variance is checked with the Goldfeld-Quandt test [16]. An additional validation is done by cross-validating the model against real historical trends. Once validated, the model can be used for forecasting future values of the time series.

III. Model identification and validation

In this work, the SARIMA identification procedure was implemented in Python using the *statsmodel* and *pmdarima* libraries to plot the required quantities and grid search for the optimal SARIMA models. Historical input data were obtained from the Geomagnetic Observatory Niemegk [17, 18], including observed and adjusted $F_{10.7}$ solar radio flux values, the eight 3-hourly a_p indices, and the daily mean A_p. These variables were subsequently post-processed for use in the NRLMSISE-00 model. The following subsections illustrate the model identification and validation process for solar and geomagnetic indices.

A. $F_{10.7}$

To apply the SARIMA model, the $F_{10.7}$ series was first preprocessed to reduce computational complexity. The original data exhibit an approximately 11-year seasonal cycle, corresponding to about 4,015 observations, which makes the identification of the seasonal parameters P and Q computationally demanding. To address this issue, monthly averaged values were used, reducing the seasonal period from 4,015 to 132 data points. This choice improves computational efficiency, although it may reduce forecast accuracy because the SARIMA model is calibrated on aggregated rather than individual observations. To reduce the data variance, a logarithmic transformation was applied. The deduced forecast trend from monthly averages is then scaled to daily units

The ADF test indicated that first-order differencing was required to achieve stationarity, while the ACF and PACF plots of the solar flux series shown in Figure 1 exhibited an early truncation pattern, suggesting the use of unitary or null model orders.

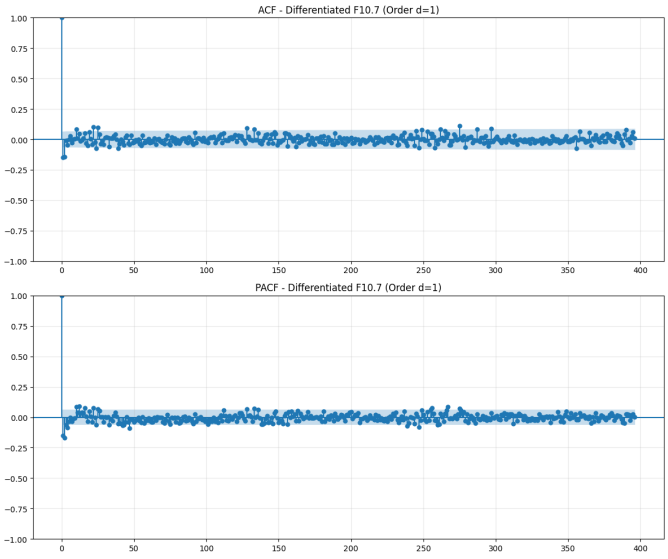

Fig. 1. ACF and PACF trends of $F_{10.7}$ time series

The following table summarizes the identified model and the corresponding test results:

SARIMA Model	$(1, 1, 1) \times (1, 1, 0, 132)$
Ljung–Box test	0.54
Jarque–Bera test	0.00
Goldfeld-Quandt test	0.04

TABLE I
IDENTIFIED SARIMA MODEL FOR THE $F_{10.7}$ SERIES.

What results from this model fitting is that the model residuals, according to the Ljung-Box test, are independent and random, due to the test value being higher than the 0.05 threshold. This means the model captured correctly the seasonal patterns and trends of the time series. On the other hand, the assumption of a normal and heteroskedastic uncertainty distribution is rejected by the Jarque-Bera and Goldfeld-Quandt tests. The cross-validation analysis further supported this conclusion by comparing the forecast uncertainty of the $F_{10.7}$ trend over the 2020-2026 interval with the corresponding observed measurements.

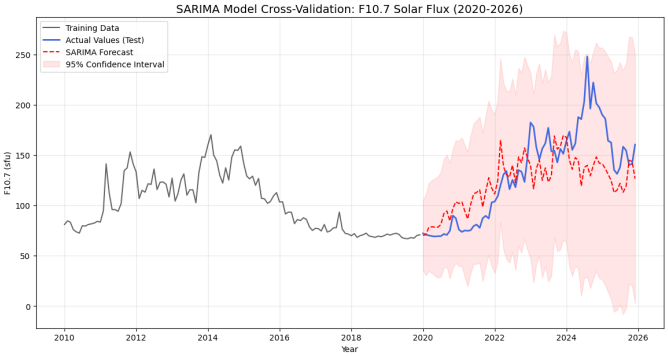

Fig. 2. Forecasted monthly averaged $F_{10.7}$ time series cross-validation in the 2020-2026 interval with normal distribution assumption

The results resumed in figure 2 showed that the uncertainty

interval obtained under the assumption of a normal distribution was excessively wide, with its lower bound extending well below historically observed minimum values, which are approximately 70 sfu.

There are indeed strong indications by NASA [19] of the fact that $F_{10.7}$ uncertainty has to be modeled using equally spaced quantiles derived from data covering the past solar cycles and creating an analog uncertainty distribution. These indications are followed, creating a past data based uncertainty range that is contained within realistic boundaries, while capturing most of actual and forecasted trends, as shown in figure 3, where most of an exceptionally high solar flux activity between 2024 and 2025 is included.

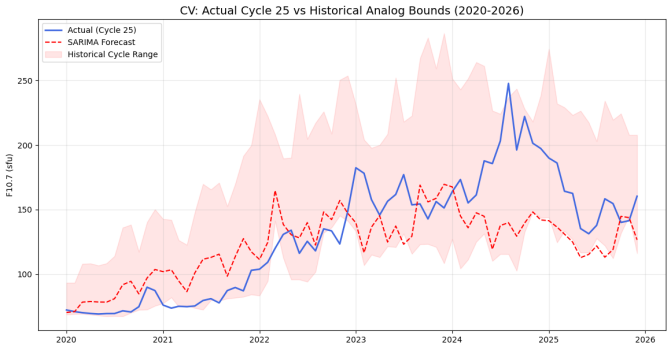

Fig. 3. Forecasted monthly averaged $F_{10.7}$ time series cross-validation in the 2020-2026 interval with pasta data based uncertainty distribution

B. A_p and a_p

The preprocessing procedure applied for $F_{10.7}$ was repeated for the average daily A_p and a_p, applying monthly averaging and logarithmic transformation. A semiannual SARIMA model was grid searched and fit through the past geomagnetic data, with the autoregressive and moving average parameters suggested by ACF and PACF plots as boundaries. As a representative case these are shown for A_p in figure 4.

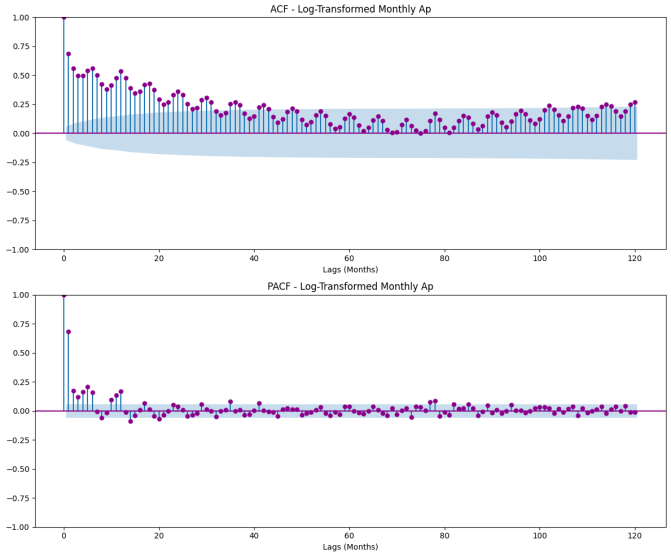

Fig. 4. A_p PACF and ACF trends

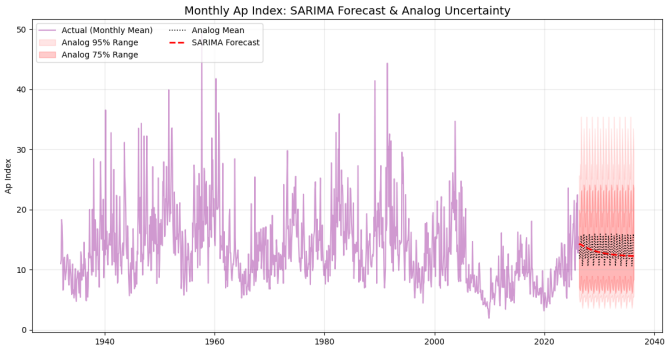

Fig. 5. A_p historical and forecasted trend with past data based uncertainties and mean

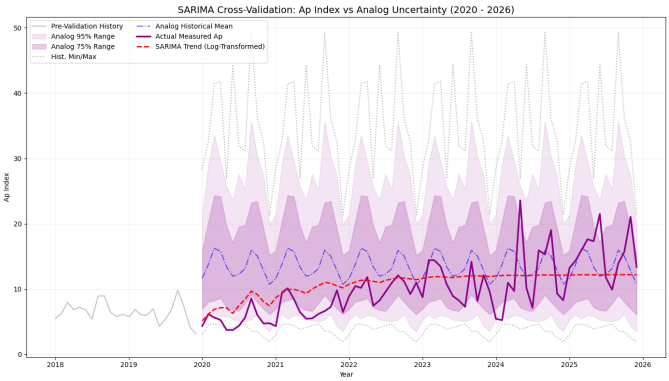

Fig. 6. Cross-validation of the A_p model

The grid search resulted in an ARIMA model that drops the seasonality assumption, and stabilizes on a constant value after a short transient. The following table summarizes the characteristics of the identified A_p model as a representative for the geoagmetic parameters, and the corresponding test results.

ARIMA Model	$(2, 0, 1)$
Ljung–Box test	0.69
Jarque–Bera test	0.03
Goldfeld-Quandt test	0.00

TABLE II
IDENTIFIED ARIMA MODEL FOR THE A_p SERIES.

Even in this case, the normal distribution hypothesis is rejected, leading to applying the NASA guidelines again on the uncertainty distribution. This lead on discovering how the constant value at which the ARIMA model settles down is around the mean of the distribution.

The cross-validation on 2020-2026 time period suggested that the model identified for this data is not fixed for every case, as for this time interval the best identified model is a SARIMA (3, 0, 0)x(2, 0, 0, 6). Nevertheless, this model aligns as well to the historical mean as the previous one, as it is shown in figure 6.

This indicates that SARIMA models, for such highly varying and stochastic time series as the geomagnetic ones, are able to suggest only a short-term varying forecast that doesn't

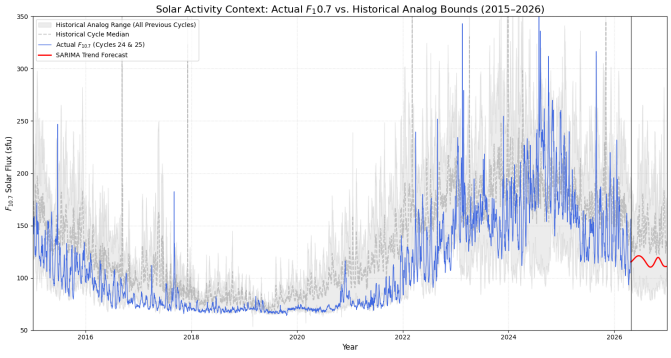

Fig. 7. Daily F10.7 measuraments in the 2015 - 2026 time interval

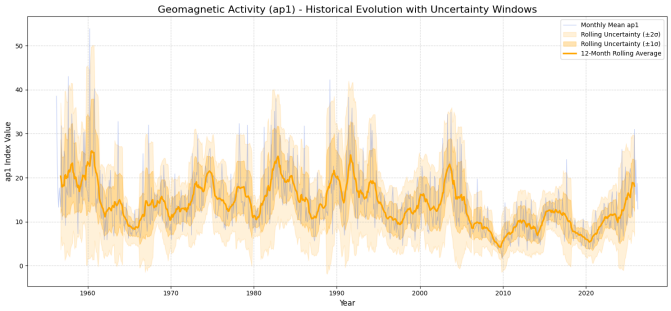

Fig. 8. Measured a_{p1} monthly average trend and uncertainty distribution

fall far from the actual measurements, while in the long-term they settle down to the average mean.

C. Scenarios definition

To compute the future air density values, it was decided to use the forecasted $F_{10.7}$ value ranges, while for A_p and hourly a_p values it was decided to discard ranges and just use the average activity. This is justified by the following considerations:

- It is reasonable to consider that the $F_{10.7}$ value can stay on the bounds of the confidence intervals for a considerable amount of time, for instance during the approach of the seasonal minima, as figure 7 shows
- On the other hand, considering A_p and hourly a_p to be on the lower edge for too much time (e.g. 5 years) it's unrealistic and would not capture the stochastic nature of this parameter, as for instance shows the monthly average historical trend of a_{p1} in figure 8. Using ranges of geomagnetic data and combining it with combining them with maximum and minimum values of $F_{10.7}$ would lead to estimate excessively low and unrealistic density values, consequently computing for instance overly conservative reentry times of an orbital decay.

This led to the definition of 3 scenarios:

1) **Low solar activity**: $F_{10.7}$ values are from the lower bound of the forecast uncertainty range
2) **Forecasted solar activity**: $F_{10.7}$ values are the forecasted by the SARIMA model
3) **High solar activity**: $F_{10.7}$ values are from the upper bound of the forecast uncertainty range

IV. Use cases

In this section, examples of the application of air density range forecasting are exposed. Two types of problems are considered:

1) **Orbital Decay**: drag, J2 and solar radiation pressure perturbed gaussian equations of motion of an uncontrolled spacecraft are propagated under every solar activity scenario, until the 150 km altitude is reached. This allows estimation of reentry time windows and compliance with 5 years limit indicated by ESA Space Debris Mitigation Requirements document [20], which integrates ECSS guidelines to support a debris-free space environment.
2) **Station-keeping**: station keeping Δv required under different solar activity scenarios is computed through the Arnas [21] approach for maintenance of Sun-Synchronous orbits.

A. Orbital Decay

An illustrative 12U CubeSat case is considered, in which the deorbiting time is compared between two scenarios: with and without the presence of a propulsion system that can lower its altitude at the end of life phase. In the following table the spacecraft characteristics assumptions are resumed:

A_{cross}	m_{dry}	c_d	c_r
0.1 m x 0.2 m	34 kg	2.2	1.3

TABLE III
12U Spacecraft assumptions

The propulsive unit considered is WaterCube+, a green hybrid propulsion system for CubeSats and small satellites, developed by a consortium led by Capsule Corporation and funded by ESA. It combines a water-based resistojet (RPM) and a hydrolysis-based module (CPM), operating in complementary thrust regimes to provide flexibility across mission requirements. The following table resumes WaterCube+ specifics:

T_{CPM}	T_{RPM}	I_s
350 mN	4 mN	110 s

TABLE IV
WaterCube+ specifics

The initial orbit considered is 400 km high circular Sun Synchronous orbit, while the time considered is when it is forecasted a low $F_{10.7}$ solar activity, leading to lower air density values and higher decay times.

a	**e**	**i**	Ω	ω	θ	**Date**
6778 km	0	97°	0°	0°	0°	1/1/2029

TABLE V
Initial orbit and time

The following altitude evolution plot shows that the initial orbit placement of the spacecraft does allow compliance to the 5 years limit only in the high solar activity scenario, showing absence of robusteness in the compliance forecast.

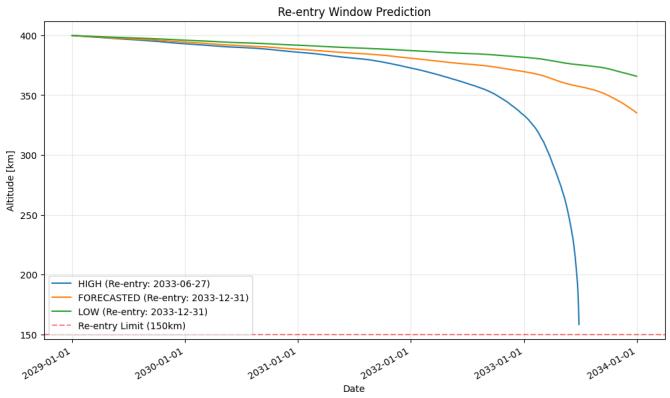

Fig. 9. Altitude time evolution from initial orbit

By assuming 1 kg of fuel on board and impulsive firings at the apogee of the orbit, it is now analysed the resulting reentry window from of the modified perigee orbit, this time having a lower perigee that allows to interact with higher density air. The modified orbit has the following Keplerian elements:

a	e	i	Ω	ω	θ	Date
6723.264 km	0.008141	97°	0°	0°	0°	1/1/2029

TABLE VI
INITIAL ORBIT AND TIME

The following plot shows how compliance to the 5 years rule is now achieved robustly, as in optimistic and pessimistic solar activity assumptions the reentry window is still compliant.

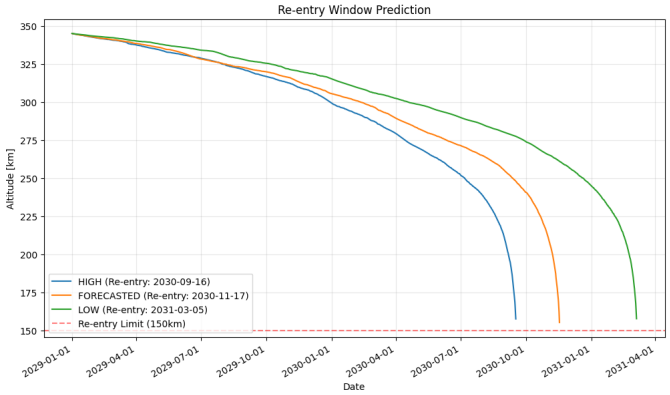

Fig. 10. Altitude time evolution from modified initial orbit with WaterCube+

B. Station-keeping

The 12U CubeSat described in Table III is analyzed under a station-keeping scenario. In this case, the spacecraft employs the WaterCube+ RPM module to perform orbit maintenance of the same initial orbit defined in Table VI. A total propellant mass of 1 kg is assumed to be available, corresponding to an overall Δv budget of 31.28 m/s.

Figure 11 illustrates the impact of different forecasted space weather scenarios, computed within a 75% confidence interval, on the achievable mission lifetime as constrained by the available Δv budget.

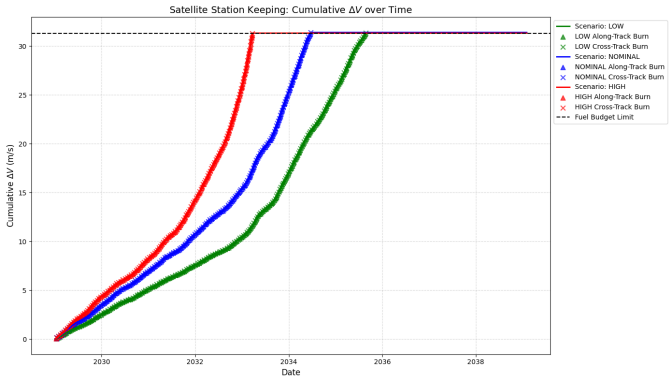

Fig. 11. Influence of different space weather scenarios on mission time

The application of this forecasting model enables the definition of a range of possible mission lifetime outcomes. This, in turn, supports mission analysts in appropriately sizing the Δv budget, while ensuring a guaranteed minimum mission duration under worst-case conditions. Such a conservative bound is represented by the high solar activity scenario, derived through the robust uncertainty quantification methodology previously described.

V. Conclusion

The application of SARIMA models to space weather indices has yielded promising results in long-term space weather forecasting. Particularly, the model demonstrates the capability to capture the seasonal trend of the $F_{10.7}$ index and to generate forecasts which, when combined with an average geomagnetic activity and with distributions derived from historical data, enable the definition of a probabilistic range of plausible space weather scenarios. This consequently allows for the computation of statistically robust ensembles of atmospheric density profiles.

As illustrated in the presented use cases, these results can effectively support mission analysts in evaluating orbit maintenance durations under Δv constraints constraints, as well as in estimating re-entry time windows. The latter is particularly relevant for verifying compliance with end-of-life disposal requirements, such as the 5-year re-entry guideline established by the ESA Space Debris Mitigation Requirements and ECSS standards.

References

[1] Qiaoli Kong, Jinyun Guo, Fan Gao, and Litao Han. Performance evaluation of three atmospheric density models on hy-2a precise orbit determination using doris range-rate data. *Journal of Testing and Evaluation*, 47(3):2150–2166, Oct 2018.

[2] Changyong He, Yang Yang, Brett Carter, Emma Kerr, Suqin Wu, Florent Deleflie, Han Cai, Kefei Zhang, Luc Sagnières, and Robert Norman. Review and comparison of empirical thermospheric mass density models. *Progress in Aerospace Sciences*, 103:31–51, 2018.

[3] A. A. Petrukovich and M. Y. Zakharov. ap-index solar wind driving function and its semiannual variations. *Annales Geophysicae*, 25(7):1465–1469, Jul 2007.

[4] Daniele Telloni. Statistical methods applied to space weather science. *Frontiers in Astronomy and Space Sciences*, 9, Jun 2022.

[5] Cong Huang, Dan-Dan Liu, and Jing-Song Wang. Forecast daily indices of solar activity, f10.7, using support vector regression method. *Research in Astronomy and Astrophysics*, 9(6):694–702, May 2009.

[6] Harry P. Warren, John T. Emmert, and Nicholas A. Crump. Linear forecasting of the f10.7 proxy for solar activity. *Space Weather*, 15(8):1039–1051, Aug 2017.

[7] Gábor Tóth, Igor V. Sokolov, Tamas I. Gombosi, David R. Chesney, C. Robert Clauer, Darren L. De Zeeuw, Kenneth C. Hansen, Kevin J. Kane, Ward B. Manchester, Robert C. Oehmke, et al. Space weather modeling framework: A new tool for the space science community. *Journal of Geophysical Research: Space Physics*, 110(A12), December 2005.

[8] Sergio Sánchez-Hurtado, William Parker, Valentin Rodríguez-Fernández, and Richard Linares. From space weather to orbits: An uncertainty-aware framework for predicting satellite trajectories. In Stefan Lemmens, Tim Flohrer, and Florian Schmitz, editors, *Proceedings of the 9th European Conference on Space Debris*. ESA Space Debris Office, 2025. Paper 377.

[9] Andong Hu and Enrico Camporeale. *A new machine learning approach for predicting extreme space weather*, Jan 2025.

[10] European Space Agency. Machine learning in support of space weather prediction – denser (deeply understanding space weather). https://tinyurl.com/4uvbx77b, 2025.

[11] Gelu M. Nita, Manolis Georgoulis, Irina Kitiashvili, Viacheslav Sadykov, Enrico Camporeale, Alexander Kosovichev, Haimin Wang, Vincent Oria, Jason Wang, Rafal Angryk, Berkay Aydin, Azim Ahmadzadeh, Xiaoli Bai, Timothy Bastian, Soukaina Filali Boubrahimi, Bin Chen, Alisdair Davey, Sheldon Fereira, Gregory Fleishman, Dale Gary, Andrew Gerrard, Gregory Hellbourg, Katherine Herbert, Jack Ireland, Egor Illarionov, Natsuha Kuroda, Qin Li, Chang Liu, Yuexin Liu, Hyomin Kim, Dustin Kempton, Ruizhe Ma, Petrus Martens, Ryan McGranaghan, Edward Semones, John Stefan, Andrey Stejko, Yaireska Collado-Vega, Meiqi Wang, Yan Xu, and Sijie Yu. Machine learning in heliophysics and space weather forecasting: A white paper of findings and recommendations. *arXiv preprint arXiv:2006.12224*, 2020.

[12] George E. P. Box, Gwilym M. Jenkins, Gregory C. Reinsel, and Greta M. Ljung. *Time Series Analysis: Forecasting and Control*. John Wiley Sons, Inc, 2016.

[13] David A. Dickey and Wayne A. Fuller. Distribution of the estimators for autoregressive time series with a unit root. *Journal of the American Statistical Association*, 74(366):427, Jun 1979.

[14] Greta M. Ljung and George E. P. Box. On a measure of lack of fit in time series models. *Biometrika*, 65(2):297–303, 1978.

[15] Carlos M. Jarque and Anil K. Bera. Efficient tests for normality, homoscedasticity and serial independence of regression residuals. *Economics Letters*, 6(3):255–259, 1980.

[16] Stephen M. Goldfeld and Richard E. Quandt. Some tests for homoscedasticity. *Journal of the American Statistical Association*, 60(310):539–547, 1965.

[17] Geomagnetic Observatory Niemegk. Kp,ap,ap,sn,f107 since 1932.

[18] J. Matzka, C. Stolle, Y. Yamazaki, O. Bronkalla, and A. Morschhauser. The geomagnetic kp index and derived indices of geomagnetic activity. *Space Weather*, 19(5), May 2021.

[19] K. Niehuss, H. Euler Jr., and W. Vaughan. Statistical technique for intermediate and long-range estimation of 13-month smoothed solar flux and geomagnetic index. NASA Technical Memorandum 4759, NASA, 1996.

[20] European Space Agency. Esa space debris mitigation requirements (essb-st-u-007, issue 1). Technical report, European Space Agency, 2021.

[21] David Arnas. Linearized model for satellite station-keeping and tandem formations under the effects of atmospheric drag. *Acta Astronautica*, 176:217–225, 2020.